



The control of short-term ice mélange weakening episodes on calving activity at major Greenland outlet glaciers

Adrien Wehrlé, Martin P. Lüthi, and Andreas Vieli

Institute of Geography, University of Zurich, 8052 Zurich, Switzerland

Correspondence: Adrien Wehrlé (adrien.wehrle@geo.uzh.ch)

Received: 18 August 2022 – Discussion started: 31 August 2022

Revised: 13 December 2022 – Accepted: 30 December 2022 – Published: 23 January 2023

Abstract. The dense mixture of iceberg of various sizes and sea ice observed in many of Greenland’s fjords, called ice mélange (*sikussak* in Greenlandic), has been shown to have a significant impact on the dynamics of several Greenland tidewater glaciers, mainly through the seasonal support it provides to the glacier terminus in winter. However, a clear understanding of shorter-term ice mélange dynamics is still lacking, mainly due to the high complexity and variability of the processes at play at the ice–ocean boundary. In this study, we use a combination of Sentinel-1 radar and Sentinel-2 optical satellite imagery to investigate in detail intra-seasonal ice mélange dynamics and its link to calving activity at three major outlet glaciers: Kangerdlugssuaq Glacier, Helheim Glacier and Sermeq Kujalleq in Kangia (Jakobshavn Isbræ). In those fjords, we identified recurrent ice mélange weakening (IMW) episodes consisting of the up-fjord propagation of a discontinuity between jam-packed and weaker ice mélange towards the glacier terminus. At a late stage, i.e., when the IMW front approaches the glacier terminus, these episodes were often correlated with the occurrence of large-scale calving events. The IMW process is particularly visible at the front of Kangerdlugssuaq Glacier and presents a cyclic behavior, such that we further analyzed IMW dynamics during the June–November period from 2018 to 2021 at this location. Throughout this period, we detected 30 IMW episodes with a recurrence time of 24 d, propagating over a median distance of 5.9 km and for 17 d, resulting in a median propagation speed of 400 m d^{-1} . We found that 87 % of the IMW episodes occurred prior to a calving event visible in spaceborne observations and that ~ 75 % of all detected calving events were preceded by an IMW episode. These results therefore present the IMW process as a clear control on the calving activity of Kangerdlugssuaq Glacier. Finally, using a

simple numerical model for ice mélange motion, we showed that a slightly biased random motion of ice floes without fluctuating external forcing can reproduce IMW events and their cyclic influence and explain observed propagation speeds. These results further support our observations in characterizing the IMW process as self-sustained through the existence of an IMW–calving feedback. This study therefore highlights the importance of short-term ice mélange dynamics in the longer-term evolution of Greenland outlet glaciers.

1 Introduction

Greenland’s ice discharge is currently contributing approximately half to the total mass loss of the ice sheet (Shepherd et al., 2020), alongside surface melt. While complex, the interactions between tidewater glaciers and the ocean have been identified as a set of key and important processes involved in Greenland’s current and future ice loss.

The high surface speed of Greenland’s major outlet glaciers coupled with sustained frontal ablation is resulting in the release of large quantities of ice in proglacial fjords. These fjords have been shaped over thousands of years by fast and concentrated ice flow and are often consisting of deep and narrow corridors. A narrow outlet combined with high ice discharge can therefore result in the congestion of icebergs in the fjords of tidewater glaciers. This dense mixture of icebergs and sea ice is commonly and hereafter called ice mélange (*sikussak* in Greenlandic).

Dense ice mélange often covers the fjords at the front of Greenland outlet glaciers, behaving like a very coarse granular material (Cassotto et al., 2021; Burton et al., 2018). Such ice covers have been identified to have high enough

yield strengths to exert back stress on glacier termini (e.g., Amundson et al., 2010a; Cassotto et al., 2015). Walter et al. (2012) estimated the back stress from winter sea-ice mélange to range from ~ 30 to 60 kPa on the entire face of the terminus of Store Glacier, corresponding to a ~ 240 –480 kPa mélange–glacier contact pressure (Todd and Christoffersen, 2014). However, such observation-based inference of mélange back stress remains scarce and results in low constraints for numerical models. Through this process, known as buttressing, ice mélange can strongly influence glacier dynamics (e.g., Dupont and Alley, 2005; Amundson et al., 2010b; Robel, 2017; Howat et al., 2010; Nick et al., 2010; Cook et al., 2014; Krug et al., 2015). At a seasonal scale, ice mélange has been shown to promote glacier advance in winter and to further leave the calving front unprotected as it breaks up in spring, leading to higher calving rates and therefore accelerated glacier retreat (Todd and Christoffersen, 2014; Moon et al., 2015; Kehrl et al., 2017; Joughin et al., 2008; Amundson and Burton, 2018).

Bevan et al. (2019) studied the variations in the position of Kangerdlugssuaq Glacier terminus in relation to fjord dynamics using satellite and reanalysis data with a focus on the period from 2011 to 2019. The authors showed that interannual warming shelf waters highly reduced the overall strength of the ice mélange, making it less efficient in inhibiting calving. In the discussion, they further identified the propagation in the up-fjord direction of one weakening wave in the ice mélange during an entire month in February–March 2018 using a series of Sentinel-1 radar images. This wave consisted of the progressive retreat of the boundary between a dense, jam-packed ice mélange strongly coupled to the calving front and a weaker, sometimes discontinuous, ice cover extending further down-fjord. Once the mass and extent of the jam-packed ice cover decreased down to a critical level at the glacier terminus, large calving events were observed. While the authors noted that this pattern is commonly seen in summer and has recently also occurred in winter, this single example only served as supporting observation for the study of interannual variations in ice mélange conditions, without further analysis.

Xie et al. (2019) studied such an ice mélange weakening (hereafter IMW) episode that occurred in June 2016 at the front of Sermeq Kujalleq in Kangia (Jakobshavn Isbræ) using a terrestrial radar interferometer. The authors focused on the retrieval of elevation changes through time, and they showed that the IMW front was characterized by an abrupt surface step change of ~ 10 m between the thick jam-packed ice mélange and the thinner and weaker ice cover extending in the down-fjord direction. This important surface drop further explains the strong contrast visible in satellite imagery across the discontinuity, e.g., in the case of the event described in Bevan et al. (2019) at Kangerdlugssuaq Glacier. Xie et al. (2019) also observed an up-fjord migration of this boundary through the occurrence of several collapse-like events, as well as the initiation of large-scale calving once the ice

mélange mass reached a critical minimum thickness and extent. This study therefore provided a high-resolution characterization of one IMW episode, complementing scarce previous work using satellite imagery.

Our knowledge of IMW episodes in Greenland and their relation to calving activity is therefore based on a highly limited number of studies. These studies mainly investigated multiannual to seasonal patterns using spaceborne observations or single events using high spatial- and temporal-resolution field measurements over short periods. A detailed assessment and characterization of short-lived IMW episodes is therefore currently missing.

In this study, we use successive Sentinel-1A and Sentinel-1B images, making the most out of its daily to 2 d revisit time over Greenland, to analyze a sample of IMW episodes at the front of three main Greenland outlet glaciers: Kangerdlugssuaq Glacier, Helheim Glacier and Sermeq Kujalleq in Kangia (Jakobshavn Isbræ). For Kangerdlugssuaq Glacier, featuring high ice mélange dynamics, we further extend our analysis to include a continuous monitoring of IMW episodes at this location during the June-to-September period from 2018 to 2021. We finally explore the drivers and controls of the IMW process using a simple numerical model for ice mélange motion. We therefore aim at improving the characterization of these short-lived events to ultimately better understand their impact on the longer-term glacier terminus stability.

2 Study sites

Kangerdlugssuaq Glacier (also known as Kangerlussuaq and hereafter referred to as KG; 68.5° N, 33.0° W) is a major outlet glacier situated in the southeastern sector of the Greenland ice sheet (Fig. 1a and c). After minor thinning from 1981 to 1998, KG thinned by ~ 100 m from 2003 to 2005 (Khan et al., 2014) and suddenly retreated by ~ 6 km in 2005, doubling its surface speed (Luckman et al., 2006). In 2011, KG slowed down and started to experience large seasonal variations of more than 3 km in its terminus position and slightly advanced by ~ 200 m until 2016 (Kehrl et al., 2017). In 2016, an almost continuous retreat was initiated. KG failed to advance in winters 2016/17 and 2017/18 (Bevan et al., 2019) and reached a terminus position unprecedented in observation records at this time (i.e., since 1932; Brough et al. (2019)). Over the past couple of years, KG seems to have returned to its pre-2016 ice discharge regime (Mankoff et al., 2020) but is still experiencing a retreat of its summer minimum front position. It currently features a ~ 5 km wide calving front which has been suggested to be close to flotation (Bevan et al., 2019). KG calves into a ~ 18 km long ~ 5 km wide secondary fjord artery, part of a 75 km long 5–10 km wide main fjord (Murray et al., 2010; Sutherland et al., 2014).

Helheim Glacier (hereafter HG; 66.4° N, 38° W), situated ~ 400 km south from KG along the southeastern Greenland coast (Fig. 1a and d), also underwent a major retreat at the beginning of the century, essentially between 2003 and 2005 (Luckman et al., 2006; Stearns and Hamilton, 2007; Howat et al., 2005, 2008). Similarly to KG, it further stabilized from 2006 until a significant increase in ice discharge was initiated in 2016 (Mankoff et al., 2020; see Fig. 1e). This regime of high discharge led HG to nearly overtake Sermeq Kujalleq in Kangia as Greenland's main ice contributor to sea level rise in early 2021, which is a pattern that currently appears to be maintained, although showing a potential decreasing trend (Mankoff et al., 2020; see Fig. 1e). HG is discharging ice into a side fjord (~ 20 km long, ~ 5.5 km wide) of the main Sermilik fjord (~ 80 km long and ~ 6 km wide; Sutherland et al., 2014). Recent research suggests that the front of HG is currently close to flotation and about to initiate a period of rapid retreat (Williams et al., 2021).

Sermeq Kujalleq in Kangia (hereafter SKK; 69.2° N, 49.6° W; Fig. 1), situated in central West Greenland (Fig. 1a and b), is among Greenland's fastest glaciers (Joughin et al., 2014). It features a ~ 25 km long calving front currently discharging more than 50 Gt of ice per year into the ocean (Mankoff et al., 2020) in the form of large icebergs which then travel through a ~ 60 km long ~ 5–12 km wide fjord before reaching Disko Bay. SKK is directly flowing into its main fjord artery to the open ocean unlike KG and HG, which first flow into secondary fjords. SKK has maintained a high flow speed of 7 km a⁻¹ since 1875 (Weidick and Bennike, 2007) before the stepwise disintegration of its floating terminus after 1997 (Sohn et al., 1998) resulted in a twofold increase in the surface velocity in the main trunk (Rignot and Kanagaratnam, 2006). After a recent slowdown linked to colder ocean waters between 2016 and 2018 (Khazendar et al., 2019), SKK has now returned to its regime of sustained mass loss since 2020.

SKK, HG and KG are currently the top three contributors to Greenland's ice discharge, accounting for 22 % of the total discharge in late September 2021 (10 %, 6 % and 5 %, respectively; Mankoff et al., 2020) and are associated with a potential sea level rise of ~ 1.3 m (Kjeldsen et al., 2015). Improving our understanding of the dynamics of those major outlet glaciers is therefore crucial to better resolve the current and future mass loss of the Greenland ice sheet.

3 Data and methods

3.1 Satellite imagery

We used Sentinel-1A and Sentinel-B synthetic-aperture radar (SAR) acquisitions of backscatter signal amplitude in polarized (horizontal–vertical; HV) and non-polarized (horizontal–horizontal; HH) modes during the June–November period from 2018 to 2021 to monitor ice

mélange conditions and dynamics at the front of the three glaciers of interest. Associated with the high latitude of the study areas, a revisit frequency from 1 to 4 d (median frequency of 1 d) was achieved, without shading from clouds to which radar satellites are immune. The combination of polarized and non-polarized modes allowed for the detection of variations in ice mélange characteristics, which could remain undetected using one mode alone. The high spatial and temporal heterogeneity of ice mélange, as well as the potential variety of processes affecting it, make the HV mode particularly useful for surface characterization. In combination with Sentinel-1 radar observations, we used Sentinel-2 optical images acquired with a frequency from 1 to 3 d over Greenland.

All satellite images used in this study were downloaded with the earthspy Python package (Wehrlé, 2023b), which is a wrapper download tool for Sentinel Hub services (Sentinel Hub, 2022).

3.2 Calving event detection

We manually detected the timing of large-scale calving events at the front of the three glaciers of interest using a combination of Sentinel-1 radar and Sentinel-2 optical data to increase temporal coverage and resolve potential detection ambiguities. We further qualitatively assigned a magnitude to each calving event in a simplified manner, depending on the detached area visible in spaceborne observations. This simple proxy for calving event magnitude could take values of 1, 2 or 3 for small-, medium- or large-size calving events, respectively.

3.3 Tracking of IMW propagation

The clear signature of IMW episodes in Sentinel-1 data at the front of KG (see videos S1 to S4, left panels, in the Supplement) allowed for a mapping of the discontinuity between jam-packed ice mélange in contact with the glacier terminus and weaker ice mélange extending further down-fjord. HG also features frequent IMW episodes every year, but their propagation is often less clearly visible and can remain ambiguous. We therefore decided to restrict the analysis at the front of HG to three well discernible IMW episodes. A similar strategy has been followed for SKK.

The results consist of a catalog of line objects corresponding to the positions of the IMW fronts through time and associated metadata (date, terminus position) for each of the three glaciers. The line objects are stored in shapefiles in the National Snow and Ice Data Center (NSIDC) Sea Ice Polar Stereographic North projection (EPSG:3413).

Manual detection was chosen after limited efforts to develop an automated detection of IMW episodes. Trials were focused on an unsupervised area classification through k-means clustering using spatial coordinates as well as Sentinel-1 backscatter amplitude in HH and HV modes as features. Performances were not satisfactory enough for the

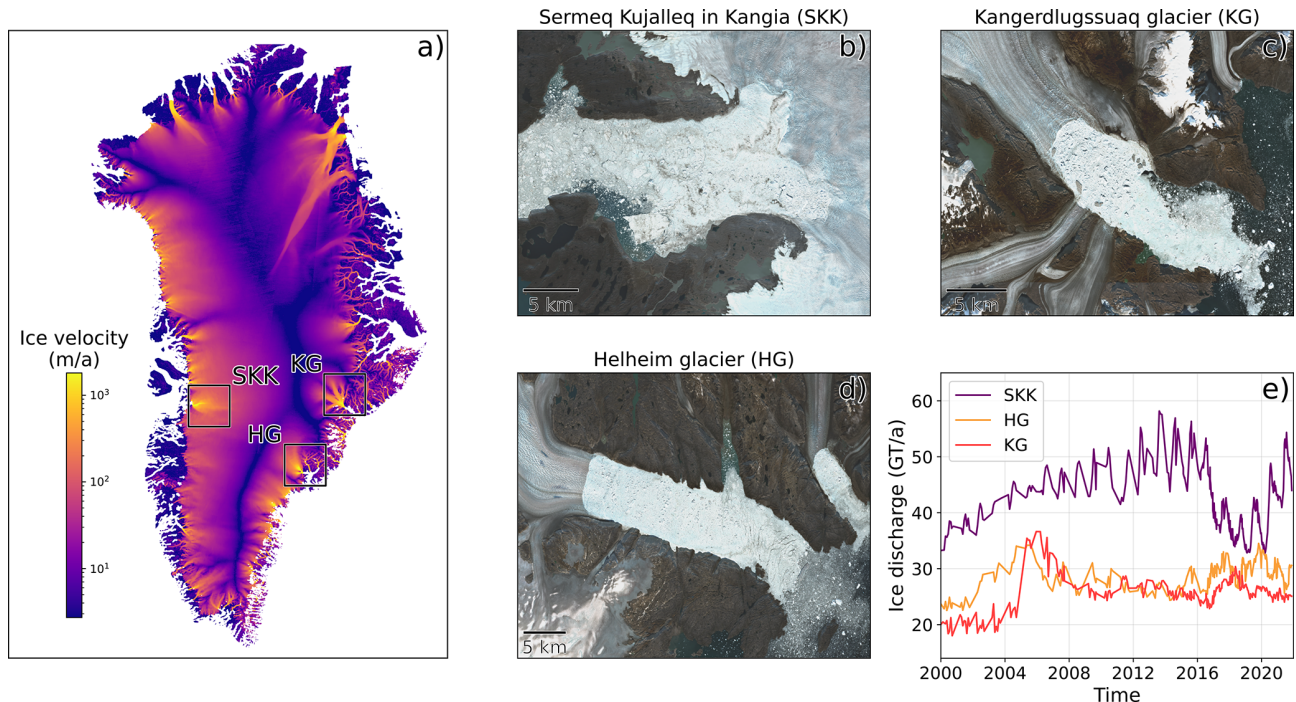


Figure 1. (a) Locations of the glaciers of interest shown on a 2020 surface velocity map of the Greenland ice sheet (Joughin, 2021). (b–d) Sentinel-2 enhanced true color images (Copernicus Sentinel data 2022, processed by ESA) of their respective calving fronts as least-cloudy mosaics in August 2020. (e) 2000–2020 respective ice discharge (Mankoff et al., 2020).

method to be used in this study, especially in complex situations which often could not be resolved with this type of surface characterization alone. Taking the dynamics of the ice mélange cover into account by adding, for example, surface velocities as another feature to distinguish between ice surface types would likely give more satisfactory results but was not further investigated here.

3.4 Biased random-walk model

To better understand the dynamics of dense ice mélange, we developed a simple numerical model based on the idea that the floating ice blocks move as in a one-dimensional Brownian random walk. This model, called BRIMM (Biased Random-walk Ice Mélange Model), is based on discrete blocks, representing floating icebergs, that move along the axis of the fjord. Blocks are created at the glacier terminus by calving and float away when they reach the end of the fjord. At each time step, each block moves by a random distance in a random direction (up-fjord or down-fjord). We ignore cohesion and momentum transfer between blocks. This means that if one block moves into another, it is simply stopped in contact with it but does not affect the position or motion of the other block.

At each model time step, all blocks move according to a random walk with uniformly distributed distance and random direction of motion (up-fjord or down-fjord). To achieve an overall down-fjord motion, a small bias is added to the ran-

dom distribution, making the blocks more likely to move away from the glacier terminus. We suggest that this bias could be the illustration of a forcing applied to the ice mélange by surface winds and/or ocean currents, specifically through subglacial freshwater discharge via meltwater plumes at the glacier front. The leftmost block, representing the advancing glacier terminus, moves at a constant speed.

The model time step size was chosen as 1/50 of a day (about 0.5 h), which is in the order of the timescale needed for acceleration and subsequent stopping of a large iceberg (see Appendix A). The maximum random motion Δx_{\max} of the blocks at each time step was varied between 10 and 80 m. The distance of random motion Δx_r was calculated by taking a value p_r from a uniform random distribution and by altering it by a bias p_b :

$$\Delta x_r = \Delta x_{\max} 2(p_r - 0.5 + p_b). \quad (1)$$

To obtain a net motion away from the calving front, a bias p_b between 0.01 and 0.11 was added to the values from the uniform random distribution p_r (between 0 and 1).

Two calving criteria were implemented to reproduce in a simple manner the fact that dense ice mélange prevents the glacier terminus from calving if the mélange is closely packed. First, calving happens when the block closest to the calving front moves a certain distance away from the front. This emulates open water between ice blocks in proximity to

the terminus and corresponds to a unconsolidated mélange without any stress transfer.

The second condition is fulfilled when within the last 5 km in front of the terminus a lead opens between two blocks that is wider than 1.5 block widths. This can be thought of as emulating the collapse of an arch structure buttressing the terminus. The length scale (5 km) corresponds to the width of the fjord since such an arch is usually shaped elliptically.

During each calving event, the glacier terminus moves back by a certain distance. A prescribed number of new ice blocks (10 to 30 in our model runs) that are initially vertical with an along-flow length of 20 m are created. During calving, the blocks turn over and extend 100 m horizontally, therefore taking up more space and pushing away blocks from the calving front that would otherwise overlap. The net effect is a dense ice mélange that extends in front of the terminus (Robel, 2017).

BRIMM is characterized by a set of parameters whose values are chosen to represent the processes in a fjord. All parameters used in this study as well as their respective ranges are shown in Table 1.

BRIMM was implemented in the Python programming language and is publicly available under the GPL-v3 license (<https://github.com/MartinLuethi/BRIMM/>, last access: 19 January 2023).

4 Results

4.1 IMW episodes at Kangerdlugssuaq Glacier

Figure 2 shows three IMW episodes propagating through jam-packed ice mélange at the front of KG. The upper panels delineate positions of the transitions between jam-packed and weak ice mélange or open ocean, color-coded for different points in time. The background Sentinel-1 HH images were acquired in the middle of each IMW episode. As the Sentinel-1 HV mode has also been used for the detection of IMW outlines when the HH mode was not sufficient, the IMW outlines do not always correspond to a clear pattern in the Sentinel-1 HH images presented here. The lower panels show the mean along-fjord distance of the IMW fronts through time. Distances were computed from a fixed on-ice reference point situated 1 km upstream of the most retreated glacier terminus position mapped in this data set.

In all three examples, the IMW front gradually propagates up-fjord in direction of the glacier terminus after a first detection close to the secondary fjord's mouth (~ 17 to 20 km from reference). Interestingly, the three IMW episodes are associated with relatively variable propagation durations (38, 25 and 32 d for the 2018, 2019 and 2021 episodes, respectively) and patterns. In the case of the 2018 and 2019 episodes, the IMW front consisted of the interface between a dense, jam-packed ice mélange (up-fjord) and a weakened ice mélange cover (down-fjord) which gradually dis-

integrated through collapse-like events. This is particularly visible on the Sentinel-1 image in Fig. 2a, where the jam-packed mélange in contact with the glacier terminus appears relatively dark, while the down-fjord area, consisting of a weak and loose ice mélange, appears lighter before the open water, featuring an almost vanishing backscatter intensity, prevails due to specular reflection. In contrast, during much of the 2021 episode the IMW front consisted of a clear-cut discontinuity between jam-packed ice mélange and open water, without a weakened ice mélange cover in between the two types of surfaces.

The 2019 and 2021 episodes feature a clear kink in the propagation curve (on 16 July 2019 and 25 September 2021, respectively; Fig. 2e and f), corresponding to a transition from fast to slower propagation around 10 km from reference. The 2018 episode (Fig. 2d) shows a more gradual propagation with a period of small position variations at the fjord mouth (23 June 2018 to 2 July 2018). For all three examples, the fastest propagation between two consecutive IMW front detections occurred when the IMW front was situated in the widest area of the fjord (10–16 km from reference), where the ice mélange is the weakest on average. Similarly, the slowest propagation speeds were observed in close vicinity of the glacier terminus (closer than 10 km from reference), where the ice mélange is thick and dense and the fjord narrower.

All three episodes were followed by a large-size (2018 and 2019) or medium-size (2021) calving event a few days after the last detection of the IMW front. These observations suggest a causal relation between the disintegration of jam-packed ice mélange and the occurrence of calving events at the front of KG. However, the impossibility to investigate subdaily glacier and fjord patterns due to the temporal resolution of the data sets used in this study prevents a detailed characterization of the transition between the terminal stage of IMW episodes and glacier calving.

4.2 IMW episodes at Helheim Glacier

Figure 3 illustrates three IMW episodes in the Sermilik fjord in front of HG. The three episodes were associated with propagation durations that are significantly shorter than at KG (17, 12 and 18 d for 2018, 2019 and 2021 episodes, respectively), and all three featured a weak ice mélange cover down-fjord from the IMW front. The 2019 and 2021 episodes show a pattern of fast up-fjord propagation and slower propagation or even stabilization closer to the glacier terminus, similar to the events presented at KG. The propagation curves feature a kink (on 8 August 2019 and 29 May 2021, respectively) but here at two different along-fjord locations ~ 3 km apart. The 2018 IMW episode shows a more gradual propagation towards the glacier terminus, similarly to the 2018 episode at KG, with a short stabilization from 21 to 24 May 2018.

In contrast to KG's fjord, HG's fjord is of relatively constant width and orientation. This setting suggests that the ice

Table 1. BRIMM parameters and their ranges explored in this study.

Parameter	Symbol	Default value	Min	Max
Length of fjord		50 km		
Length of floating block		100 m		
Length of block before calving		20 m		
Flow speed of the glacier terminus		15 m d^{-1}		
Number of tracked floating blocks		300		
Number of calving blocks		20	10	30
Length of terminus retreat after calving		$20 \cdot 20 = 400 \text{ m}$	$10 \cdot 20 \text{ m}$	$30 \cdot 20 \text{ m}$
Random walk time step	Δt	0.02 d		
Maximum random walk step length	Δx_{max}	50 m	10	80
Random walk bias	p_b	0.02	0.01	0.11
Calving criterion 1: width of lead		20 m		
Calving criterion 2: width of lead		150 m		

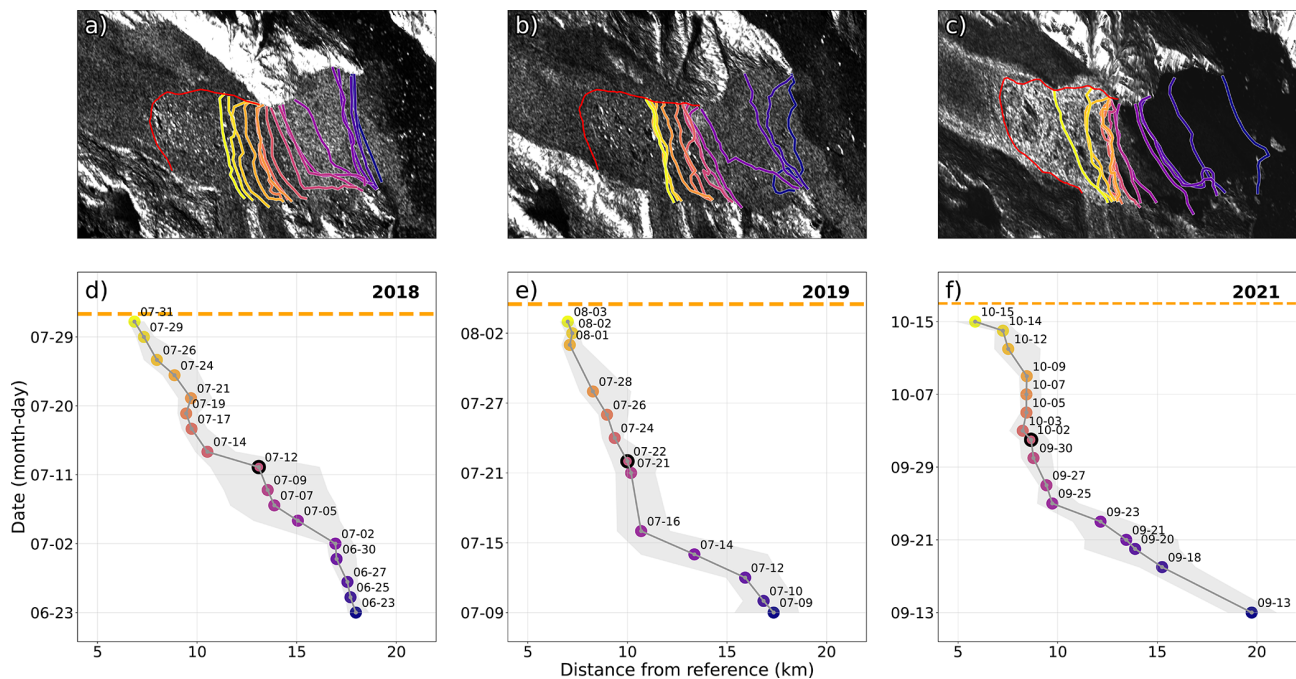


Figure 2. Three IMW episodes at KG. (a–c) Positions of the IMW fronts through time in Cartesian coordinates, overlaying Sentinel-1 HH images acquired half-way through each IMW episode (Copernicus Sentinel data 2022, processed by ESA). Red lines correspond to the position of the calving front. (d–f) Distance between IMW fronts and an on-ice reference situated 1 km upstream from the most retreated glacier terminus position mapped in the data set. Dot color corresponds to each IMW front mapped in (a)–(c) through time and black dot contours to the acquisition dates of the respective Sentinel-1 HH images. The gray curves indicate the median along-fjord distance of the IMW front from the on-ice reference. The envelopes correspond to the range between minimum and maximum along-fjord distance at each time steps (therefore quantifying the across-fjord variations in IMW front position). Horizontal orange dashed lines indicate the timing of calving events detected with spaceborne observations, with their width being proportional to their approximated magnitude (small, medium or large). Time is running from bottom up.

mélange strength and density contribute more to the IMW dynamics at HG than at KG. The fjord at HG is, however, connected to a secondary artery on its northern shore, which alters the ice mélange structure. This impact is visible through the pinning of the IMW front on this crossing point (Fig. 3a–c) at the beginning of the 2019 and 2021 episodes

(5 August 2019 and 26 May 2021) and in the middle of the 2018 episode (21 to 24 May 2018).

In a manner similar to KG, large calving events followed the last detection of the IMW front at HG. However, small calving events occurred during the IMW episodes (one in 2019 and 2021; two in 2018) at HG in contrast to KG. This

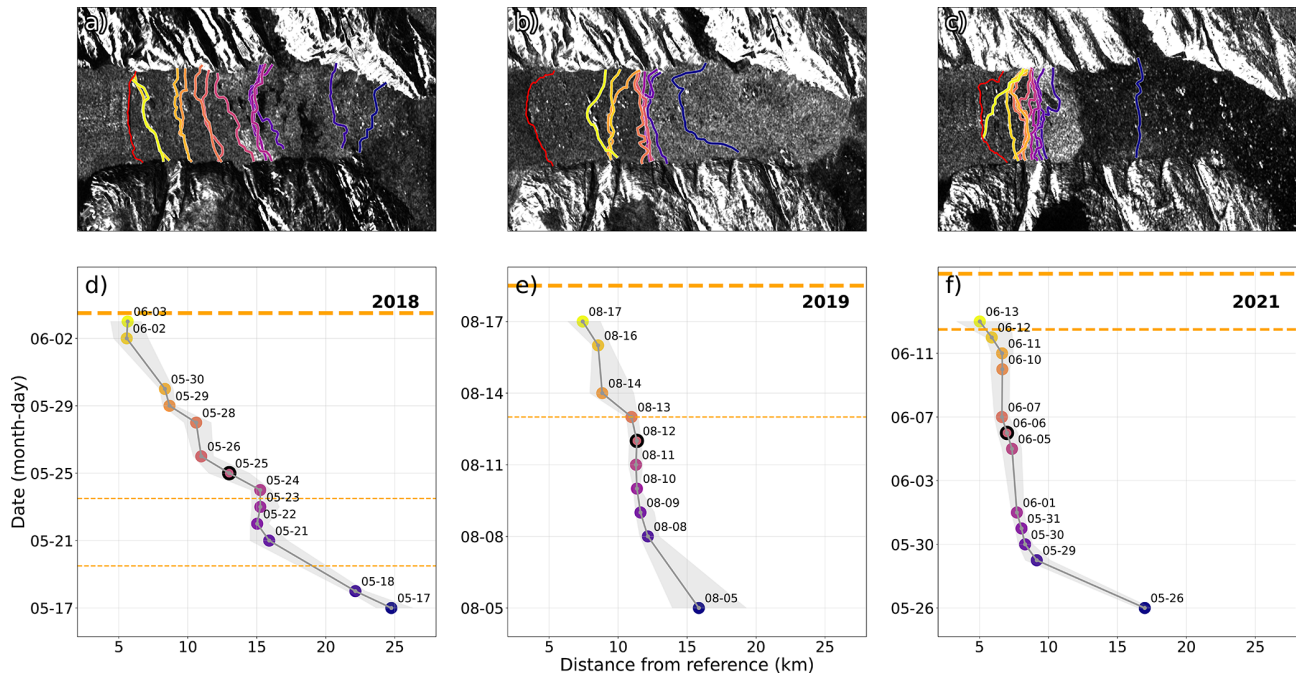


Figure 3. Three IMW episodes at HG presented in the same manner as in Fig. 2. See caption of Fig. 2 for details.

might suggest that the IMW process exerts less control on calving activity at the front of HG compared to KG.

4.3 IMW episodes at Sermeq Kujalleq in Kangia

Figure 4 shows the propagation of three IMW episodes at the front of SKK. These three episodes show a wider variety of propagation characteristics than the events analyzed at KG and HG. Propagation durations of 10, 27 and 65 d were determined (for the first and second episode of 2018 and the 2021 episode, respectively), therefore showing a large range of 55 d.

The first 2018 IMW episode featured a very clear up-fjord weakening propagation associated with IMW fronts of low complexity and limited across-fjord kinking. This episode ended only 4 d before the beginning of the second 2018 episode which was almost 3 times shorter (10 d) but also showed a clearly visible propagation. During both episodes, the dense ice mélange covering an embayment on the southern shore of the fjord remained unaffected. The 2021 episode shows more complex IMW front outlines which may be linked to the breakup of the ice mélange in the embayment area, suddenly increasing the distance between the two lateral pinning points and therefore most likely contributing to a more variable and unstable discontinuity.

In the case of the first 2018 episode and the 2021 episode, a kink in the propagation curve is again visible (on 11 May 2018 and 29 July 2021) but this time with the fastest propagation occurring in the vicinity of the glacier terminus, unlike the events presented at KG and HG. In the case of

the second 2018 episode and the 2021 episode, the Sentinel-1 images in the middle of the two events show the formation of two polynyas (open water, visible as dark areas surrounded by ice mélange) on the southern and northern fjord shores, respectively. The polynyas were formed right in front of the IMW discontinuity, highlighting a strong decoupling between areas of dense and weaker ice mélange.

Similarly to KG and HG, large-size (first episode in 2018 and 2021 episode) and medium-size (second episode in 2018) calving events occurred at the end of the respective IMW episodes. In the case of the 2021 episode, a medium-size calving event occurred in the early stage of the weakening propagation.

4.4 Continuous IMW episode analysis at Kangerdlugssuaq Glacier

To better understand the main characteristics of the IMW episodes in the KG fjord, IMW fronts were tracked continuously during the June–November periods of the years 2018 to 2021. This monitoring shows a highly dynamic proglacial ice cover during summer and fall.

Black lines in Fig. 5 show the along-fjord propagation of IMW fronts in a similar manner as in Figs. 2 to 4. The IMW episodes displayed in Fig. 2 are highlighted with red vertical bars. Orange horizontal lines indicate calving events visible in satellite imagery, as well as an estimate of their magnitude.

During the study period of four summer and fall seasons, a total of 30 IMW episodes were observed. The propagation of the associated IMW fronts is clearly visible in the animations

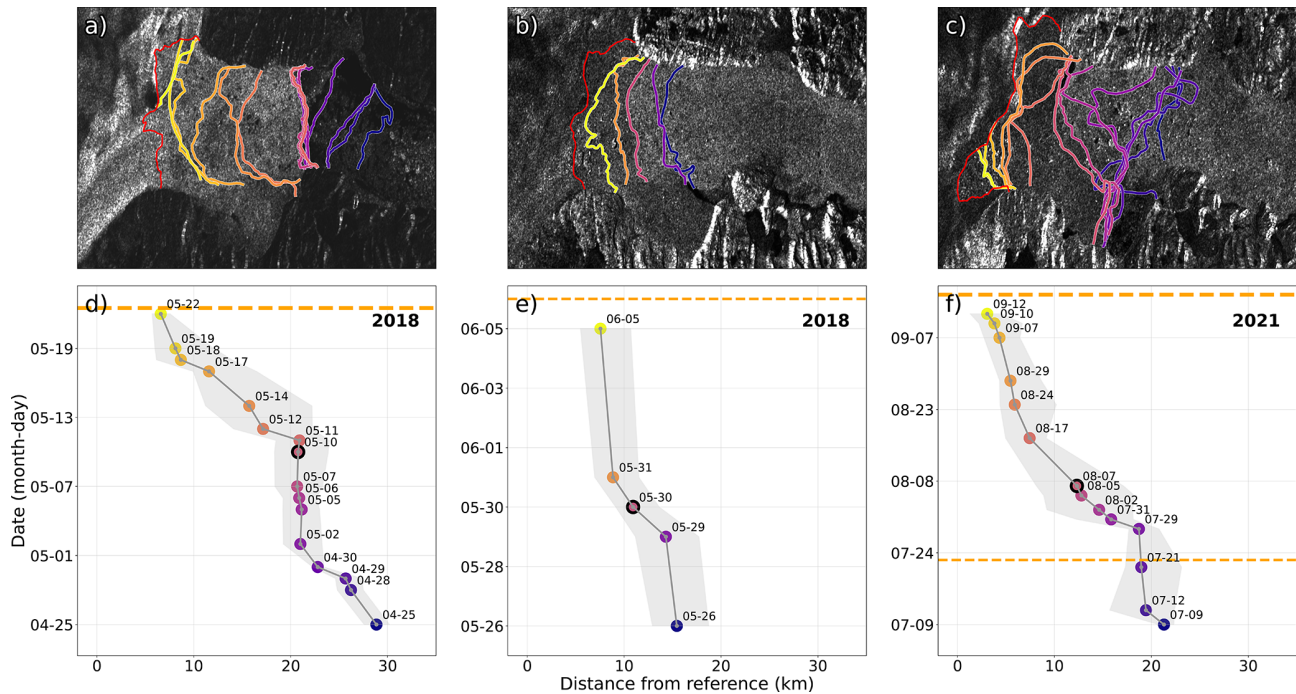


Figure 4. Three IMW episodes at SKK presented in the same manner as in Fig. 2. See caption of Fig. 2 for details. The Sentinel-1 HH images have been flipped horizontally to keep the right-to-left convention for IMW propagation direction.

(videos S1 to S4 from 2018 to 2021). Five to 8 IMW episodes were detected per season (June to November), corresponding to an average recurrence time of 24 ± 3 d. In parallel, 37 calving events were detected using spaceborne observations with an average of 9 ± 1 events per season. Combining the IMW tracking with calving event detection, we found that 87 % of the IMW episodes were closely followed by a calving event. Conversely, we found that 70 % of detected calving events occurred subsequent to an IMW episode. Assuming that IMW episodes can have a cascade effect and also including calving events occurring a few days after the IMW-triggered calving events, this ratio increases up to 81 %. An example of this cascade effect is late November 2020 (see Fig. 5c).

Using our simple proxy for calving magnitude, we found that from 78 % to 90 % of the cumulated calving magnitude over the study period was released following an IMW episode. While the strong link between calving activity and the termination of IMW episodes seems clear, the calving inhibition during those episodes is even more pronounced. Only 16 % of the calving events occurred during an IMW episode before the IMW front reached the glacier terminus, and only 7 % of the cumulated calving magnitude was released during IMW episodes.

Focusing on intra-episode characteristics, a recurrent pattern (45 % of all IMW episodes) of fast propagation speeds at the early stage of the episodes (down-fjord) and slower propagation speeds at the end of the episode (in the vicinity of

the glacier terminus) were observed. Such a pattern was already identified in the 2019 and 2021 episodes presented in Fig. 2. Three IMW episodes (June 2019, October 2019 and November 2020) featured a two-stage propagation without calving. The first IMW front stabilized mid-fjord at around 9 km (June and October 2019) and 5 km (November 2020) from the reference point and was further overtaken a few days later by a second and faster IMW front. No calving event was detected following the intermediate stabilization.

Winter IMW activity was low in 3 of the 4 years spanning the study period, with the notable exception of winter 2018/19. In winters 2019/20, 2020/21 and 2021/22 no IMW episodes and only rare calving events were observed. The ice mélange remained tightly coupled to the glacier terminus which was continuously advancing. In winter 2018/19 IMW episodes occurred without any interruption from the end of our continuous monitoring (late November) to its beginning the following year (early June). During this period, the calving activity showed a similar relation to IMW episodes as during the spring-to-fall period.

These strong interannual variations in winter ice mélange dynamics are likely due to starkly different meteorological conditions. In winters 2019/20, 2020/21 and 2021/21 sea ice remained dense and almost motionless in the fjord for 108–152 d (~ 120 d from 2 February to 2 June 2019; ~ 108 d from 15 February to 2 June 2020; ~ 152 d from 18 January to 19 June 2021). In contrast, no dense sea ice formed at the

fjord scale during the entire winter 2018/19, and the ice cover remained relatively mobile.

4.5 IMW characteristics

Figure 6 presents several variables characterizing IMW episodes: propagation distance, duration and propagation speed. Quantities for the three IMW episodes studied at KG, HG and SKK (Figs. 2–4) are shown with colored dots. The distributions obtained from 30 IMW episodes analyzed at KG (Fig. 5) are shown as violin plots (gray areas). The second IMW episode detected in 2021 (Fig. 5d) is not shown in Fig. 6c due to its anomalously high propagation speed (3.4 km in 1 d), which would have highly altered and flattened the visualization of the probability density function. This episode nevertheless still contributes to the median propagation speed.

The median propagation distance determined at KG was 5.9 km for a median propagation duration of 17 d, with a wide spread of values from 1 to 52 d. The median propagation speed was 400 m d^{-1} with a significant variability between 100 and 1200 m d^{-1} . The three IMW episodes of Fig. 2 illustrate the high end of propagation distances at KG (10.3 to 13.9 km) and show propagation duration values that are also above the median but lower than the maximum (25 to 38 d for a maximum of 52 d). The resulting propagation speeds remain close to the median (variations from +30 to -100 m d^{-1} around median).

While the three isolated IMW episodes studied at HG and SKK cannot give any clear insight into the distribution of the propagation characteristics at the front of these glaciers, they still illustrate possible situations that can be compared to the extended detection at KG.

The six IMW episodes at SKK and HG featured higher propagation distances than the median distance computed at KG (from 7.7 to 22.1 km) with three events (two at SKK, one at HG) above KG's maximum of 13.9 km. The propagation durations of the three IMW episodes at HG are relatively close to KG's median duration (from 12 to 18 d) while the IMW episodes at SKK show a wider spread (from 8 to 65 d). Five out of six IMW episodes show higher propagation speeds than KG's median, and one episode at SKK (9 July 2021) was associated with a lower speed of 300 m d^{-1} . Similarly to the maximum propagation distance and duration (22.1 km and 65 d), the overall maximum propagation speed (1.5 km d^{-1}) was recorded for an IMW episode that occurred at SKK. The geometry of SKK's fjord (significantly longer and wider than KG's and HG's fjords) can explain higher propagation distances and durations at this glacier. The conditions to obtain higher propagation speeds might be linked to a lower ice mélange cohesion at SKK than at KG and HG, but they remain mostly unclear at this point.

4.6 BRIMM results

BRIMM was run with a set of geometrical and model parameters that are inspired by the physical characteristics observed at KG and SKK (Fig. 6) and which were varied in ranges corresponding to realistic values (Table 1). The model, based on a random walk of discrete blocks, shows emergent dynamics that resemble observations (see videos S5 to S7). The results show iceberg jamming in the fjord after calving; IMW episodes with realistic propagation speeds of the weakening front; and quasi-periodic, punctuated dynamics. By variation of two model parameters, different dynamical characteristics emerge that allow us to better understand the processes controlling ice-choked fjords.

For all model runs, a fixed number of 300 blocks, representing floating icebergs, was used, although not all blocks are always within the fjord of 50 km length. The number of blocks released from the glacier at each calving event was set to 10 (or 20, 30). This corresponds to a glacier retreat of 200 m (or 400, 600 m) at each calving event, assuming that blocks are 20 m long before calving. We further assume that all blocks rotate during calving and occupy an along-flow length of 100 m, therefore adding 1000 m (or 2000, 3000 m) of floating icebergs to the fjord in front of the terminus.

From the model experiments, we found that the parameters Δx_{max} and p_b (Eq. 1) are the most important controls of the emergent dynamics. The maximum random motion at each time step Δx_{max} quantifies the agility of the ice mélange. The random bias p_b controls how much the random motion is directed out of the fjord and away from the glacier terminus. In what follows, all model results are shown for variations of these two parameters.

Figures 7 and 8 show BRIMM results in a manner similar to Fig. 5. Clearly, the frequency of calving events depends crucially on both Δx_{max} and p_b . With increasing random motion per time step, the frequency of calving events increases. Higher mobility of the blocks decreases the density of the ice mélange and therefore leads to more open water close to the terminus, triggering calving events according to our model assumptions. Similarly, a higher random bias moves the icebergs at a faster speed away from the glacier terminus, again leading to more open water and more frequent calving.

Several quantities that can be compared to observations were extracted from BRIMM results: the average advance rate of the glacier terminus position, the propagation speed of IMW fronts, the frequency of calving events and the mean duration of the IMW episodes. Comparing these quantities to observations allows us to determine model parameters that reproduce realistic dynamics. Figure 9 shows these characteristic quantities color-coded for variations of the model parameters Δx_{max} and p_b . Black lines indicate the observed ranges from Fig. 6.

The most important prerequisite for a calving glacier in a fjord is a relatively stable terminus position (otherwise there would be a glacier extending to the fjord mouth or no glacier

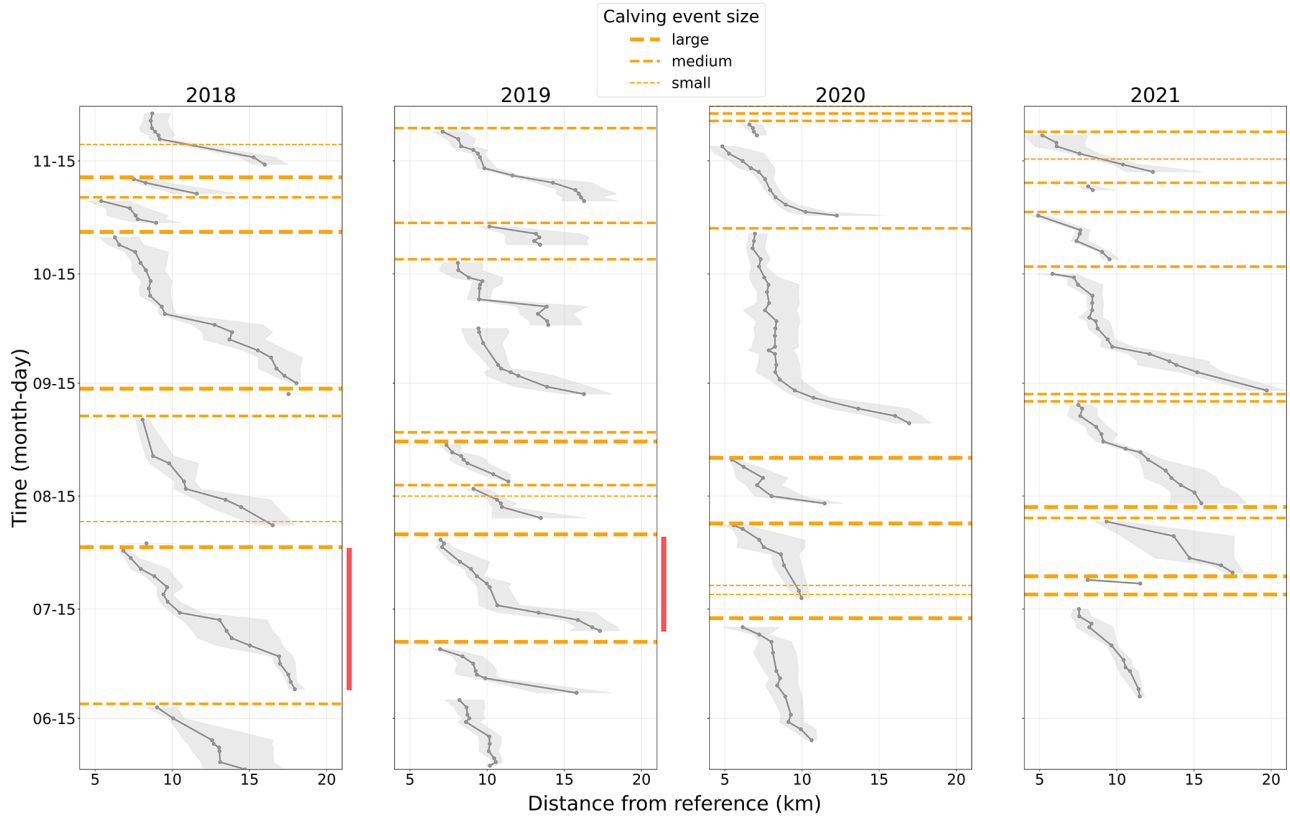


Figure 5. Detection and tracking of IMW episodes at KG during the June–November period from 2018 to 2021 presented in a similar manner as in Figs. 2 to 4. The three vertical red bars indicate the three IMW episodes presented in Fig. 2.

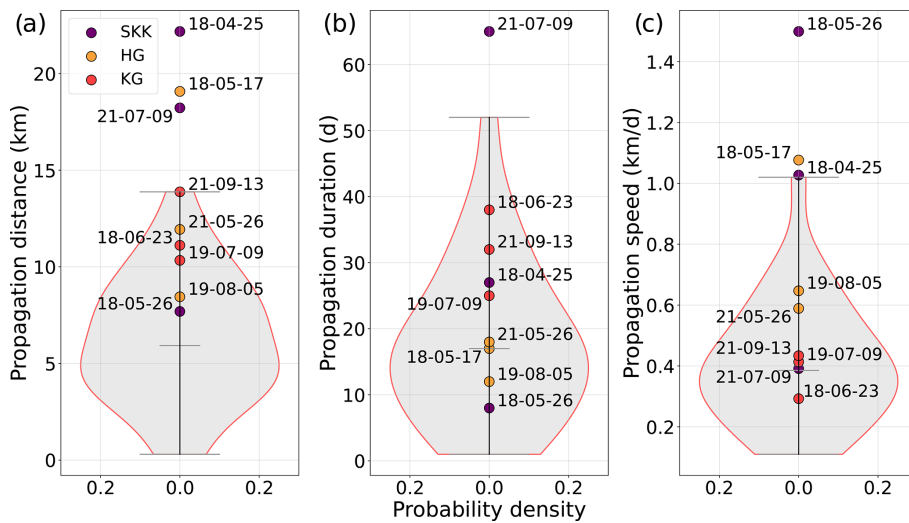


Figure 6. (a) Propagation distance, (b) duration and (c) speed of 29 IMW episodes detected at KG, presented as mirrored probability density functions, also known as violin plots (gray areas). The central tick corresponds to the median and the upper and lower ones to the distribution’s extrema. The second IMW episode detected in 2021 (Fig. 5) has been removed from (c) due to its anomalously high propagation speed (3.4 km in 1 d), which would have highly altered the representation of the probability density function. This episode nevertheless still contributes to the variable’s statistics. The characteristics of each set of three IMW episodes analyzed at KG, HG and SKK and presented in Figs. 2 to 4 are shown as red, orange and purple dots, respectively.

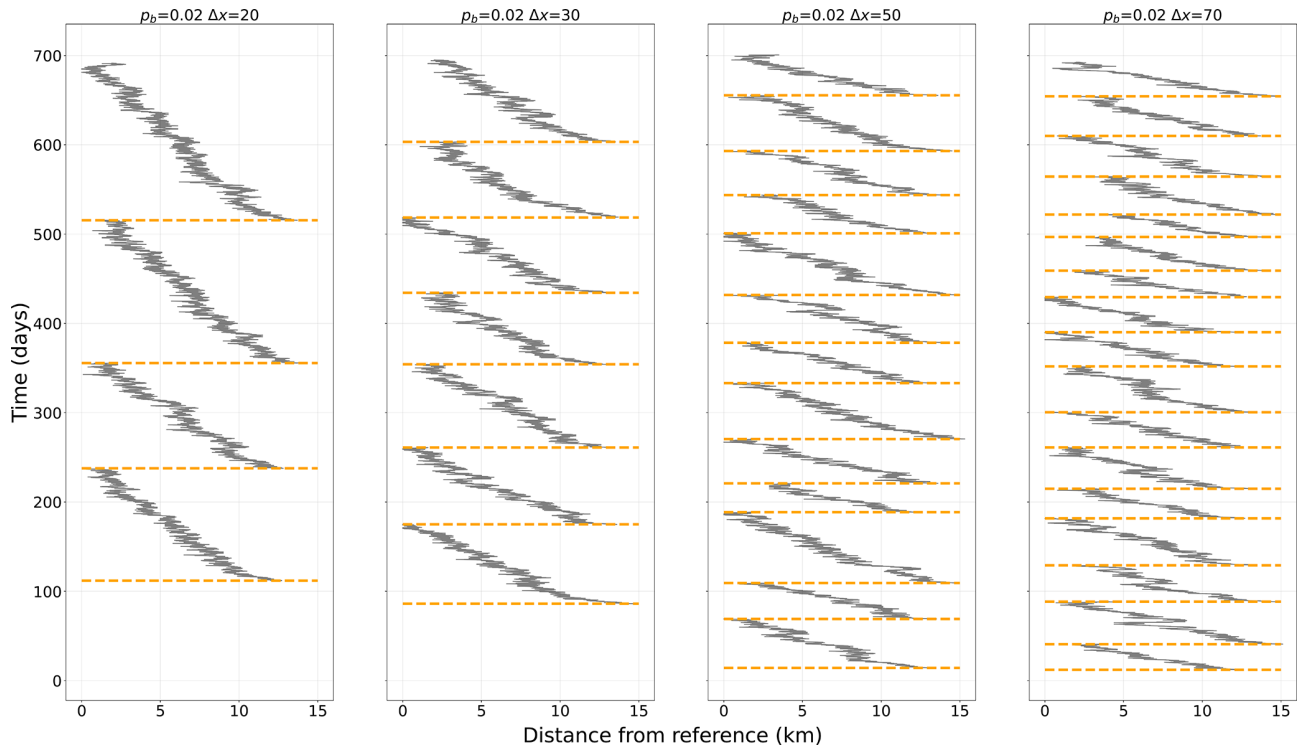


Figure 7. Along-fjord propagation of IMW fronts as modeled by BRIMM. In each panel a different value of maximum random motion Δx_{\max} is used.

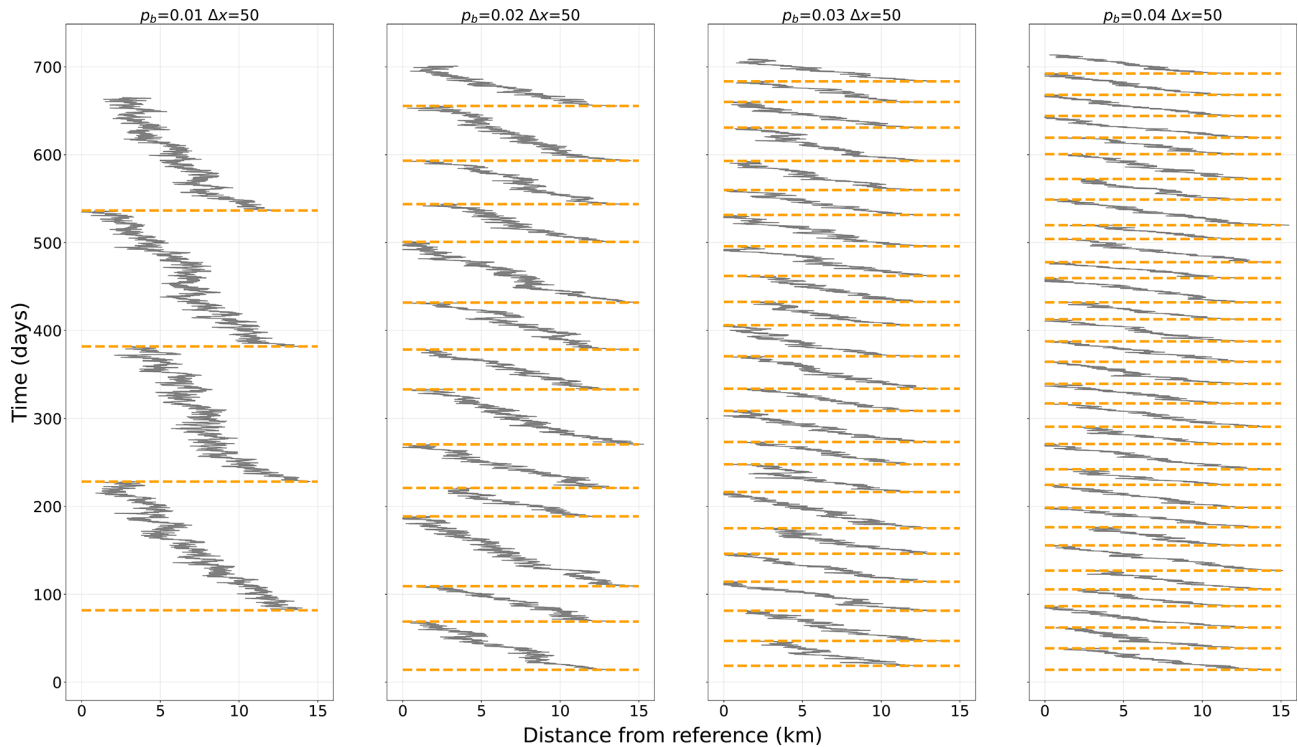


Figure 8. Along-fjord propagation of IMW fronts as modeled by BRIMM. In each panel a different value of the random bias p_b is used.

at all). Figure 9a shows that a stable terminus position (i.e., a terminus advance rate close to zero) is only achieved for certain combinations of random motion Δx_{\max} and bias p_b . These two quantities are complementary in the sense that a larger random bias requires a smaller random motion for a stable terminus position and vice versa. Similar conclusions can be drawn from the IMW propagation speed (Fig. 9b) and the average duration of an IMW episode (Fig. 9c).

5 Discussion

Through the inspection of Sentinel-1 and Sentinel-2 spaceborne observations at the terminus of SKK, HG and KG, we analyzed a set of IMW episodes and linked them to the timing of large-scale calving events. Our results conclusively show that dense, jam-packed ice mélange is an efficient short-term calving inhibitor. Removing or weakening this dense ice mélange in front of the glacier terminus by a propagating IMW front releases the inhibitor and therefore effectively triggers calving. In this sense, the IMW process can be understood as an important control on calving activity.

5.1 Self-sustained IMW cycle

While the role played by dense ice mélange in inhibiting calving at the seasonal scale has been discussed before (e.g., Walter et al., 2012; Cassotto et al., 2015; Bevan et al., 2019; Cook et al., 2014) and still receives a lot of attention, the general absence of calving events during the cyclic propagation of successive IMW fronts over the summer period appears as a more complex relation and raises important questions.

How can the ice mélange initially inhibit and by its disintegration trigger calving in a cyclic manner throughout the season? Why is its influence not suppressed after the first IMW episode? In other words, how can a weakened ice mélange switch back to its strong inhibiting behavior?

Based on our observations and the results from BRIMM, we suggest that the jam-packed ice mélange initially plays a similar role at short timescales as observed in seasonal patterns until it reaches a minimum length close to the glacier terminus. At this stage, the suppression of calving by the ice mélange is no longer strong enough to prevent calving events that would have been ready to occur without such a support. The subsequent calving events lead to large stress variations at the glacier terminus, potentially leading to a cascade effect such that secondary calving events may eventually occur, as observed at KG (Fig. 5).

The switch back to a strongly inhibiting behavior of the ice mélange and the resetting of its distribution within the fjord are needed for the next IMW episode to occur. We suggest that the resetting is initiated by the calving event itself. Each calving event releases large amounts of floating ice into the fjord, thus strengthening the ice mélange in front of the

terminus (Xie et al., 2019). Relaxation within this dense ice forces the expansion of a spatially constrained ice cover and therefore increases its density and cohesion. Although any input of ice into the fjord would result in an expansion of the ice cover, calved ice blocks that are not experiencing capsizing after detachment have a limited impact as their area at the fjord surface remains the same after calving. On the other hand, buoyancy-driven calving events, as well as chunks of ice with a low length-to-height ratio before detachment, have the strongest jamming effect as their capsizing strongly increases their area at the fjord surface. Such capsizing icebergs are frequently observed at the fronts of major Greenland outlet glaciers which are close to flotation and reside in very deep fjords. In addition, the continuous advance of the glacier terminus also promotes the densification of the proglacial ice mélange.

Associated with its slow expansion following a calving event, the ice mélange can lose its cohesion, forcing its yielding, starting at the down-fjord boundary: a new IMW episode is therefore initiated. Using a discrete element model to simulate mélange as a cohesive granular material, Robel (2017) showed that the occurrence of calving events initiates a propagating jamming wave within the mélange (in the down-fjord direction, opposite to IMW episodes), causing a local compression and slow mélange expansion over several hours before the ice mélange would slowly return to the background rate of glacier advance over the next few days. The authors further describe this jamming wave as the trigger of widespread fractures in the sea ice. This result further supports our hypothesis that calving is resetting the dense ice mélange and further forcing its yielding, thus sustaining the IMW process.

We therefore suggest that the intra-seasonal IMW process remains self-sustained following the spring onset and until winter conditions prevail. The latter condition might never be attained as exemplified in the exceptionally warm winter 2018 when the IMW process never shut down at KG. This cyclic behavior therefore consists of an IMW–calving feedback where IMW episodes control the timing of calving events, and calving events reset the fjord to conditions triggering the next IMW episodes.

5.2 Prerequisites for the IMW process

In order to better understand whether IMW episodes play a role at other outlet glaciers, we qualitatively inspected ice mélange dynamics in a large selection of Greenland outlet glaciers.

The main initial condition for IMW episodes is the sustained presence of a dense ice mélange. Such dense, jam-packed ice mélange could only be observed at the front of fast outlet glaciers discharging into relatively narrow fjords. We therefore suggest that the formation of such a dense ice mélange is best promoted when high ice discharge into the fjord is combined with a narrow outlet, limiting the evac-

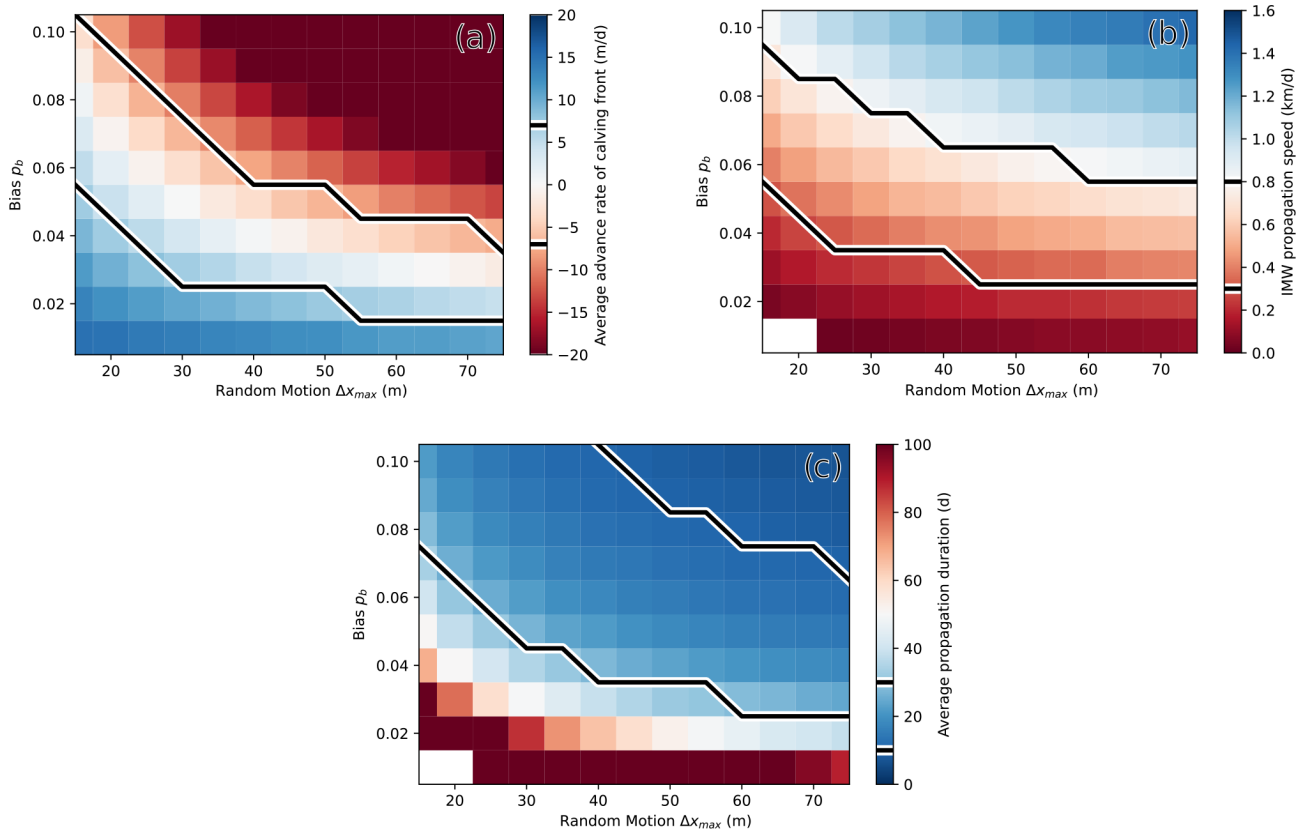


Figure 9. Dependence of observable quantities in BRIMM on model parameters Δx_{\max} and p_b . Black lines indicate the upper and lower ranges of observed values from Fig. 6.

uation of floating ice to the open ocean. Many Greenland outlet glaciers, while associated with a high ice discharge, mostly fail at retaining icebergs all year long. These glaciers, such as Eqip Sermia, are flowing into a fjord that is not narrow enough with respect to the incoming ice flux to create a dense ice cover. We also suggest that there is no absolute value of fjord geometry and ice discharge for the formation of dense ice mélangé but rather different combinations of parameters. This implies that a ratio between solid ice discharge and a fjord's narrowness might give valuable insight into ice mélangé conditions at a given location. For a more realistic representation, the dependence of ice mélangé density on air and ocean temperature should be included. It is noteworthy that hardly any dense ice mélangé was observed in southern Greenland, where the temperatures are the highest on average. Combining these three primary parameters, the three glaciers of interest in this study appear as clear candidates for the presence of a dense ice mélangé cover, which is supported by in situ and remote sensing observations. More specifically, KG emerges as the best candidate as it features the highest ratio of discharge to fjord width. KG is also the glacier in our selection featuring the most frequent and clearest IMW episodes. This suggests that the higher the ice jamming, the clearer the IMW patterns. While we presented here what we

consider as the primary conditions for the formation of dense ice mélangé, we acknowledge that the latter also depends on ocean temperatures as well as on iceberg size distributions, most likely among many other factors.

A search for IMW episodes in a large selection of outlet glaciers around Greenland yields interesting results. Clear IMW episodes were found at Alison Glacier, Upernavik Isstrøm, Sverdrup Glacier, Fenris Glacier, Nansen Glacier, Anoritup Kangerlua and in Mogens Heinesen Fjord. While the IMW process is clearly observable, the IMW activity at these glaciers is lower than at KG, with a number of events comparable to HG and SKK. We suggest that this observation is mainly linked to the conditions for dense ice mélangé discussed above, which are only partially met at those locations.

With a better insight into the conditions for a sustained dense ice mélangé and a wider view of IMW dynamics around Greenland, it is now important to discuss the actual drivers of IMW episodes. Bevan et al. (2019) showed that the recent interannual ice mélangé dynamics at KG were strongly impacted by the warming of shelf waters. Here, we used the ERA5 global reanalysis (Hersbach et al., 2020) in search for environmental parameters influencing the shorter-term ice mélangé dynamics at the IMW episode scale. We

analyzed air temperature, wind direction and wind speed as well as sea surface temperature variations, wave heights and tides at the mouth of KG's fjord and could not find patterns matching the timing, duration (17 d on average) or frequency (average recurrence time of 24 d) of the IMW episodes presented in this study, and this was with or without time lags. Further comparing the conditions at the onset of IMW episodes with the average seasonal conditions during the study period using a Student's t test, we did not find any statistically significant differences. This absence of relation might be linked to ERA5's incapacity to resolve the smaller-scale dynamics along the coast of Greenland due to its resolution of 30 km. The use of higher-resolution data sets or in situ measurements might unravel potential relations so far hidden. On the other hand, a persistent lack of evidence for external forcing might suggest IMW dynamics are mostly driven by variations in the internal state of the ice mélange.

5.3 Drivers of IMW episodes

To understand the main drivers for IMW episodes, we employed a stochastic model of iceberg motion in a fjord. With the help of BRIMM, our simple 1D iceberg dynamics model, we were able to reproduce IMW episodes that are similar to those observed in satellite imagery. The aim of investigations with such a simple model is evidently not the realistic reproduction of real-world events. Rather, BRIMM facilitates the investigation of the relative importance of different processes, and it is used for an assessment of the sensibility to different choices of model parameters, the length and timescales, and the emerging dynamics. BRIMM produces a wide variety of responses, mainly depending on the magnitude, time interval and bias of the random iceberg motion.

In the BRIMM simulations, the amount of random motion in the fjord depends on the number of time steps and on the distance of random iceberg motion Δx_{\max} . In addition, the biased preferential motion (due to p_b) away from the glacier terminus dictates the flux of icebergs through the fjord and therefore strongly influences the density of floating icebergs.

An oscillating but long-term stable terminus position is only occurring in a limited range of model parameters. To achieve this dynamical equilibrium, a prerequisite is that the rate of iceberg release from the glacier and the rate of iceberg transport by the biased random walk are of similar magnitude.

If the iceberg released to the fjord is too small (calving events of small size) and the fjord currents (p_b in the model) rapidly carry away the icebergs, no dense ice mélange can develop. Without dense ice mélange, calving is occurring continuously, and its rate is fully determined by processes at the calving front. In deep water, the ice front rapidly recedes until it reaches a shallower pinning point (not used in the model runs shown here). Such a setting applies to many Greenland fjords and has been well documented in the bay in front of Equip Sermia (e.g., Walter et al., 2020; Wehrlé et al., 2021).

If, on the other hand, iceberg release to the fjord is too high (many calving events, large iceberg volumes released), paired with a low mobility of floating icebergs, the fjord becomes densely packed, and newly calved icebergs and glacier advance preclude the formation of open water leads. Such packed ice mélange slows down IMW episodes, which are often stopped halfway up the fjord, and therefore suppresses calving. In such a setting, the ice mélange occupies large parts of the fjord, and the glacier advances through the fjord until it stagnates in the vicinity of the fjord mouth, where the open ocean will facilitate frequent IMW events that stabilize the terminus position.

5.4 Timescales

Several timescales dominate the ice mélange dynamics. The one important assumption – implemented in BRIMM – is that calving is only possible if a narrow open water lead reaches the glacier terminus or if a wide open lead forms at a certain distance (5 km in our model runs) from the terminus. We assume that the timescales intrinsic to the glacier which control calving are much faster than ice mélange weakening dynamics. We therefore assume that the glacier is always ready to calve, as soon as an open water lead forms in the vicinity of the calving front.

Under these assumptions, the only timescale dictated by glacier dynamics is the rate of terminus advance, i.e., the glacier speed. Its effect on the ice mélange is restricted to pushing floating icebergs ahead of the calving front, therefore forming a dense proglacial ice mélange that precludes calving. The rate of glacier motion in large outlet glaciers in Greenland is between 5 and 40 m d⁻¹. This means that the extent of a typical iceberg (100 m in our model runs) is covered within 3 to 20 d. In our model runs, we chose a terminus advance speed of 15 m d⁻¹.

The other important timescale is related to the random motion of the ice mélange. It is given by the frequency with which icebergs move a random distance in a random direction (up-fjord or down-fjord), which corresponds to a time step in BRIMM. Based on arguments given below, we assume in our model runs that an iceberg moves 50 times a day according to Eq. (1). This randomness is biased away from the glacier by p_b , representing ocean currents and wind drift in the real world.

Icebergs move mostly by seemingly random motion, driven by currents within the fjord and by wind forcing (Fitz-Maurice et al., 2016). Strong tidal currents exert important drag forces on icebergs (Hughes, 2022) and drive them back and forth twice daily. The alternating flow of tides every 6 h gives a good upper limit of the timescale for the random motion (i.e., 0.25 d). Fjord seiches, i.e., long-period waves within the fjord, move at wave speeds such that they have a recurrence time of about 30 min (i.e., 0.02 d; Amundson et al., 2008).

An alternative line of reasoning considers how long it takes to accelerate and to stop an iceberg of 100 m length (see Appendix A). Given the viscosity of water and the drag coefficient, a characteristic length scale Λ of roughly the size of the iceberg (i.e., 100 m) is obtained. This means that the stopping distance of a moving iceberg is about 2.3Λ . Assuming the iceberg initially moves at 1 m s^{-1} , the stopping timescale is 100 s. The acceleration of an iceberg will be of similar magnitude given that the accelerating force has to be at least twice the drag force in water. Therefore the acceleration of an iceberg and the deceleration need some 500–1000 s. This simple argument shows that during a day there cannot be more than 100 random motions. Again, an iceberg motion time step of 0.01–0.02 d emerges. Based on the above arguments, we used a time step size of $1/50 \text{ d} = 0.02 \text{ d}$ for the BRIMM runs, i.e., each iceberg moves twice per hour in a random direction by a random distance.

The ice mélange dynamics generated by BRIMM are not matching the observed behavior in much detail. But by changing a few more parameters, a much more chaotic response could be achieved. For example, the number of calving blocks could be varied either randomly or dependent on proglacial ice mélange thickness.

6 Conclusions

The analysis of spaceborne observations in combination with model results suggest that the IMW process is an important control on the calving activity of KG and to a lesser extent at HG and SKK. While the dense ice mélange cover at the front of the glacier efficiently inhibits calving during the early stage of an IMW episode, the final stage of such an episode triggers large-scale calving events. Results from a numerical model suggest that the observed cyclic IMW process is self-sustained and controlled by an IMW–calving feedback. Through this feedback, late-stage IMW episodes trigger new calving events, while the calving promotes the compaction and eventual yield of the ice mélange, thus giving rise to new IMW episodes.

An important conclusion from the modeling study is that slightly biased random motion of icebergs is sufficient to explain observed IMW dynamics. No fluctuating external forcing is needed to explain the cyclic behavior, the progress of IMW episodes or the observed IMW propagation speeds. The observed ice mélange dynamics can be explained by random motion, with an emergent behavior of self-sustained punctuated dynamics, which is reminiscent of self-organized criticality (SOC; e.g., Jensen, 1998).

This study demonstrates the importance of short-term ice mélange dynamics for the calving activity of large Greenland outlet glaciers. While radar satellite imagery provides an almost daily revisit time over the entire ice sheet, the scale of the patterns it can resolve – both spatially and temporally – remains limited compared to high-resolution field acqui-

sitions that, however, are often of short duration. More and longer in situ measurements are therefore needed to bridge this observational gap.

The study also underlines the importance of properly understanding the dynamics of floating icebergs, especially their disintegration and melting due to heat advected by ocean currents in a fjord. Observing ice mélange conditions is very difficult, but it is a prerequisite for predicting the future evolution of ice mélange dynamics around Greenland in the context of climate change. Newly established states will likely result in a strong and tight competition between processes affecting the cohesion of dense ice mélange, such as enhanced surface and submarine melt due to higher temperatures, and those promoting its spread and strengthening, which is mainly an intensification of fjord jamming due to a higher ice discharge.

A better understanding of such a complex, dynamic and heterogeneous environment can therefore only be achieved through a combination of different complementary observational and numerical approaches. Such an effort will eventually help with resolving the influence of current and future ice mélange dynamics on the longer-term stability of Greenland outlet glaciers.

Appendix A

BRIMM assumes a random motion distance from 10 to 80 m and a corresponding timescale $\Delta t = 0.02 \text{ d} \sim 30 \text{ min}$. Here, we give a rationale for choosing these values for the model parameters (following <https://physics.stackexchange.com/questions/72503/how-do-i-calculate-the-distance-a-ship-will-take-to-stop>, last access: 19 January 2023).

An iceberg moving at a speed v is slowed down by drag forces in the water. For an iceberg of mass M , Newton's second law gives

$$M \frac{dv}{dt} = -F_{\text{drag}}. \quad (\text{A1})$$

The drag force is given by

$$F_{\text{drag}} = \frac{1}{2} C_D \rho_w v^2 A, \quad (\text{A2})$$

where $C_D \sim 0.9$ is the commonly assumed drag coefficient (Lu et al., 2021; Eik, 2009) and A is the cross section under water. Writing the iceberg mass as $M = \rho_i A L$ (and therefore assuming a rectangular-shaped iceberg) and using the definition of a stopping length scale,

$$\Lambda = \frac{2M}{C_D \rho_w A} = \frac{2L \rho_i}{C_D \rho_w} = 2 \frac{0.9}{C_D} L \sim 2L, \quad (\text{A3})$$

leads to the dynamic equation

$$\frac{dv}{dt} = \frac{-1}{\Lambda} v^2. \quad (\text{A4})$$

Integration gives $v(t) = \Lambda/(t + t_0)$ with integration constant t_0 chosen such that the ratio Λ/t_0 matches the initial speed v_0 of the iceberg; that is, $t_0 = \Lambda/v_0$. The distance traveled is the integral over $v(t)x(t) = \Lambda \ln \frac{t+t_0}{t_0}$.

For an iceberg of length $L = 100$ m, as assumed in our BRIMM runs, the length scale is $\Lambda \sim 200$ m, and with an initial speed of 1 m s^{-1} $t_0 \sim 200$ s. Reducing the speed by 90 % takes $9t_0$ and therefore roughly half an hour, corresponding to our chosen time step size. The iceberg will have moved $\ln(10)\Lambda \sim 2.3\Lambda \sim 230$ m during this time.

The length and timescales established above pertain to an iceberg slowing down without any external influence. In the BRIMM runs, we assume that the forcing is randomly changing in strength and direction (backwards or forwards). Therefore, the icebergs do not have the time needed to decelerate completely to a standstill.

This discussion does not, and cannot, provide any stringent arguments for the chosen time step Δt and the maximum random motion distance Δx_{max} . On the other hand, the chosen values are of mutually compatible magnitude and lay within reasonable limits.

Code availability. The version of the earthspy Python package used to process and download Sentinel-1 and Sentinel-2 images for this study is presented in a Zenodo repository: <https://doi.org/10.5281/zenodo.7498876> (Wehrlé, 2023a). The latest earthspy version can be installed from <https://github.com/AdrienWehrle/earthspy> (last access: 19 January 2023; Wehrlé, 2023b). The version of BRIMM used in this study is presented in a Zenodo repository: <https://doi.org/10.5281/zenodo.7548884> (Lüthi, 2023a). The latest version of BRIMM is available at <https://github.com/MartinLuethi/BRIMM> (last access: 19 January 2023; Lüthi, 2023b).

Data availability. Sentinel-1 and Sentinel-2 satellite data are freely available on the ESA Open Access Hub (ESA, 2022). All IMW fronts analyzed in this study have been publicly shared as shapefiles in a Zenodo repository: <https://doi.org/10.5281/zenodo.7499245> (Wehrlé, 2023c).

Supplement. S1 to S4: animations of Sentinel-1 HH images at KG showing the migration of IMW fronts (red lines) for the June–November period from 2018 to 2021. The overlaying red lines were removed on the left panels to fully appreciate the discontinuity between jam-packed and weak ice mélange. Early in the season and towards the outer part of the fjord, dense and weak ice mélange and open water respectively appear as dark and light gray, and black due to different surface characteristics. S5 to S7: animations of BRIMM results obtained with the parameter values listed in Table 1, twenty calving blocks, a length of terminus retreat after calving of 400 m, a random walk bias of 0.02, and a maximum random walk step length of 20, 100, and 150 m for S5, S6, and S7, respectively. Light blue, dark blue and white areas represent the glacier, open water and ice mélange, respectively. The red line shows the

position of the open water lead that is the closest to the glacier terminus. The y dimension has been expanded for visualization purposes only. The supplement related to this article is available online at: <https://doi.org/10.5194/tc-17-309-2023-supplement>.

Author contributions. AW initiated the study with support from MPL and performed the analysis of satellite images. MPL developed and analyzed BRIMM. AW and MPL drafted the paper. All authors contributed to the editing and reviewing of the paper. All authors have read and agreed to the published version of the paper.

Competing interests. The contact author has declared that none of the authors has any competing interests.

Disclaimer. Publisher's note: Copernicus Publications remains neutral with regard to jurisdictional claims in published maps and institutional affiliations.

Financial support. This research has been supported by the Schweizerischer Nationalfonds zur Förderung der Wissenschaftlichen Forschung (grant no. 200020_197015).

Review statement. This paper was edited by Christian Haas and reviewed by Suzanne Bevan and Surui Xie.

References

- Amundson, J., Truffer, M., Lüthi, M. P., Fahnestock, M., Motyka, R. J., and West, M.: Glacier, fjord, and seismic response to recent large calving events, Jakobshavn Isbræ, Greenland, *Geophys. Res. Lett.*, 35, L22501, <https://doi.org/10.1029/2008GL035281>, 2008.
- Amundson, J. M. and Burton, J. C.: Quasi-Static Granular Flow of Ice Mélange, *J. Geophys. Res.-Earth Surf.*, 123, 2243–2257, <https://doi.org/10.1029/2018jf004685>, 2018.
- Amundson, J. M., Fahnestock, M., Truffer, M., Brown, J., Lüthi, M., and Motyka, R.: Ice mélange dynamics and implications for terminus stability, Jakobshavn Isbræ, Greenland, *J. Geophys. Res.*, 115, F01005, <https://doi.org/10.1029/2009JF001405>, 2010a.
- Amundson, J. M., Fahnestock, M., Truffer, M., Brown, J., Lüthi, M. P., and Motyka, R. J.: Ice mélange dynamics and implications for terminus stability, Jakobshavn Isbræ, Greenland, *J. Geophys. Res.*, 115, F01005, <https://doi.org/10.1029/2009JF001405>, 2010b.
- Bevan, S. L., Luckman, A. J., Benn, D. I., Cowton, T., and Todd, J.: Impact of warming shelf waters on ice mélange and terminus retreat at a large SE Greenland glacier, *The Cryosphere*, 13, 2303–2315, <https://doi.org/10.5194/tc-13-2303-2019>, 2019.
- Brough, S., Carr, J. R., Ross, N., and Lea, J. M.: Exceptional Retreat of Kangerlussuaq Glacier, East Greenland, Between 2016 and 2018, *Front. Earth Sci.*, 7, 123, <https://doi.org/10.3389/feart.2019.00123>, 2019.

- Burton, J. C., Amundson, J. M., Cassotto, R., Kuo, C.-C., and Denzin, M.: Quantifying Flow and Stress in Ice mélange, the World's Largest Granular Material, *P. Natl. Acad. Sci. USA*, 115, 5105–5110, <https://doi.org/10.1073/pnas.1715136115>, 2018.
- Cassotto, R., Fahnestock, M., Amundson, J. M., Truffer, M., and Joughin, I.: Seasonal and Interannual Variations in Ice Melange and Its Impact on Terminus Stability, *Jakobshavn Isbræ, Greenland, J. Glaciol.*, 61, 76–88, <https://doi.org/10.3189/2015jog13j235>, 2015.
- Cassotto, R. K., Burton, J. C., Amundson, J. M., Fahnestock, M. A., and Truffer, M.: Granular decoherence precedes ice mélange failure and glacier calving at Jakobshavn Isbræ, *Nat. Geosci.*, 14, 417–422, 2021.
- Cook, S., Rutt, I. C., Murray, T., Luckman, A., Zwinger, T., Selmes, N., Goldsack, A., and James, T. D.: Modelling environmental influences on calving at Helheim Glacier in eastern Greenland, *The Cryosphere*, 8, 827–841, <https://doi.org/10.5194/tc-8-827-2014>, 2014.
- Dupont, T. and Alley, R.: Assessment of the importance of ice-shelf buttressing to ice-sheet flow, *Geophys. Res. Lett.*, 32, L04503, <https://doi.org/10.1029/2004GL022024>, 2005.
- Eik, K.: Iceberg drift modelling and validation of applied meteorological hindcast data, *Cold Reg. Sci. Technol.*, 57, 67–90, <https://doi.org/10.1016/j.coldregions.2009.02.009>, 2009.
- ESA: Copernicus Sentinel data, <https://scihub.copernicus.eu> (last access: 19 January 2023), 2022.
- FitzMaurice, A., Straneo, F., Cenedese, C., and Andres, M.: Effect of a sheared flow on iceberg motion and melting, *Geophys. Res. Lett.*, 43, 12–520, <https://doi.org/10.1002/2016gl071602>, 2016.
- Hersbach, H., Bell, B., Berrisford, P., Hirahara, S., Horányi, A., Muñoz-Sabater, J., Nicolas, J., Peubey, C., Radu, R., Schepers, D., Simmons, A., Soci, C., Abdalla, S., Abellan, X., Balsamo, G., Bechtold, P., Biavati, G., Bidlot, J., Bonavita, M., Chiara, G., Dahlgren, P., Dee, D., Diamantakis, M., Dragani, R., Flemming, J., Forbes, R., Fuentes, M., Geer, A., Haimberger, L., Healy, S., Hogan, R. J., Hólm, E., Janisková, M., Keeley, S., Laloyaux, P., Lopez, P., Lupu, C., Radnoti, G., Rosnay, P., Rozum, I., Vamborg, F., Villaume, S., and Thépaut, J.: The ERA5 global reanalysis, *Q. J. Roy. Meteor. Soc.*, 146, 1999–2049, <https://doi.org/10.1002/qj.3803>, 2020.
- Howat, I. M., Joughin, I., Tulaczyk, S., and Gogineni, S.: Rapid retreat and acceleration of Helheim Glacier, east Greenland, *Geophys. Res. Lett.*, 32, L22502, <https://doi.org/10.1029/2005GL024737>, 2005.
- Howat, I. M., Joughin, I., Fahnestock, M., Smith, B. E., and Scambos, T. A.: Synchronous retreat and acceleration of southeast Greenland outlet glaciers 2000–06: ice dynamics and coupling to climate, *J. Glaciol.*, 54, 646–660, 2008.
- Howat, I. M., Box, J. E., Ahn, Y., Herrington, A., and McFadden, E. M.: Seasonal variability in the dynamics of marine-terminating outlet glaciers in Greenland, *J. Glaciol.*, 56, 601–613, <https://doi.org/10.3189/002214310793146232>, 2010.
- Hughes, K. G.: Pathways, Form Drag, and Turbulence in Simulations of an Ocean Flowing Through an Ice Mélange, *J. Geophys. Res.-Oceans*, 127, e2021JC018228, <https://doi.org/10.1029/2021jc018228>, 2022.
- Jensen, H. J.: Self-Organized Criticality, Lecture notes in Physics, Cambridge University Press, 1998.
- Joughin: MEaSURES Greenland 6 and 12 day Ice Sheet Velocity Mosaics from SAR, Version 1, Boulder, Colorado USA, NASA National Snow and Ice Data Center Distributed Active Archive Center [data set], <https://doi.org/10.5067/6JKYGMZOZFYJ>, 2021.
- Joughin, I., Howat, I. M., Fahnestock, M., Smith, B., Krabill, W., Alley, R. B., Stern, H., and Truffer, M.: Continued evolution of Jakobshavn Isbræ following its rapid speedup, *J. Geophys. Res.*, 113, F04006, <https://doi.org/10.1029/2008JF001023>, 2008.
- Joughin, I., Smith, B. E., Shean, D. E., and Floricioiu, D.: Brief Communication: Further summer speedup of Jakobshavn Isbræ, *The Cryosphere*, 8, 209–214, <https://doi.org/10.5194/tc-8-209-2014>, 2014.
- Kehrl, L. M., Joughin, I., Shean, D. E., Floricioiu, D., and Krieger, L.: Seasonal and interannual variabilities in terminus position, glacier velocity, and surface elevation at Helheim and Kangerlussuaq Glaciers from 2008 to 2016, *J. Geophys. Res.-Earth Surf.*, 122, 1635–1652, 2017.
- Khan, S. A., Kjeldsen, K. K., Kjær, K. H., Bevan, S., Luckman, A., Aschwanden, A., Bjørk, A. A., Korsgaard, N. J., Box, J. E., van den Broeke, M., van Dam, T. M., and Fitzner, A.: Glacier dynamics at Helheim and Kangerdlugssuaq glaciers, southeast Greenland, since the Little Ice Age, *The Cryosphere*, 8, 1497–1507, <https://doi.org/10.5194/tc-8-1497-2014>, 2014.
- Khazendar, A., Fenty, I. G., Carroll, D., Gardner, A., Lee, C. M., Fukumori, I., Wang, O., Zhang, H., Seroussi, H., Moller, D., Noël, B. P. Y., van den Broeke, M. R., Dinardo, S., and Willis, J.: Interruption of two decades of Jakobshavn Isbræ acceleration and thinning as regional ocean cools, *Nat. Geosci.*, 12, 277–283, <https://doi.org/10.1038/s41561-019-0329-3>, 2019.
- Kjeldsen, K. K., Korsgaard, N. J., Bjørk, A. A., Khan, S. A., Box, J. E., Funder, S., Larsen, N. K., Bamber, J. L., Colgan, W., van den Broeke, M., Siggaard-Andersen, M.-L., Nuth, C., Schomacker, A., Andresen, C. S., Willerslev, E., and Kjær, K. H.: Spatial and Temporal Distribution of Mass Loss From the Greenland Ice Sheet Since AD 1900, *Nature*, 528, 396–400, <https://doi.org/10.1038/nature16183>, 2015.
- Krug, J., Durand, G., Gagliardini, O., and Weiss, J.: Modelling the impact of submarine frontal melting and ice mélange on glacier dynamics, *The Cryosphere*, 9, 989–1003, <https://doi.org/10.5194/tc-9-989-2015>, 2015.
- Lu, W., Amdahl, J., Lubbad, R., Yu, Z., and Løset, S.: Glacial ice impacts: Part I: Wave-driven motion and small glacial ice feature impacts, *Marine Struct.*, 75, 102850, <https://doi.org/10.1016/j.marstruc.2020.102850>, 2021.
- Luckman, A., Murray, T., de Lange, R., and Hanna, E.: Rapid and synchronous ice-dynamic changes in East Greenland, *Geophys. Res. Lett.*, 33, L03503, <https://doi.org/10.1029/2005GL025428>, 2006.
- Lüthi, M. P.: BRIMM, a simple fjord melange dynamics model (srht/master github/master e3ae4f91446e28b94b28b131b59e8a8fd756f8af), Zenodo [code], <https://doi.org/10.5281/zenodo.7548884>, 2023a.
- Lüthi, M. P.: BRIMM, <https://github.com/MartinLuethi/BRIMM>, GitHub [code], last access: 19 January 2023b.
- Mankoff, K. D., Solgaard, A., Colgan, W., Ahlstrøm, A. P., Khan, S. A., and Fausto, R. S.: Greenland Ice Sheet solid ice discharge from 1986 through March 2020, *Earth Syst. Sci. Data*, 12, 1367–1383, <https://doi.org/10.5194/essd-12-1367-2020>, 2020.

- Moon, T., Joughin, I., and Smith, B.: Seasonal to multiyear variability of glacier surface velocity, terminus position, and sea ice/ice mélange in northwest Greenland, *J. Geophys. Res.-Earth Surf.*, 120, 818–833, 2015.
- Murray, T., Scharrer, K., James, T. D., Dye, S. R., Hanna, E., Booth, A. D., Selmes, N., Luckman, A., Hughes, A. L. C., Cook, S., and Huybrechts, P.: Ocean regulation hypothesis for glacier dynamics in southeast Greenland and implications for ice sheet mass changes, *J. Geophys. Res.*, 115, F3, <https://doi.org/10.1029/2009jf001522>, 2010.
- Nick, F., Van der Veen, C., Vieli, A., and Benn, D.: A physically based calving model applied to marine outlet glaciers and implications for the glacier dynamics, *J. Glaciol.*, 56, 781–794, 2010.
- Rignot, E. and Kanagaratnam, P.: Changes in the Velocity Structure of the Greenland Ice Sheet, *Science*, 311, 986–990, <https://doi.org/10.1126/science.1121381>, 2006.
- Robel, A. A.: Thinning sea ice weakens buttressing force of ice-berg mélange and promotes calving, *Nat. Commun.*, 8, 1–7, <https://doi.org/10.1038/ncomms14596>, 2017.
- Sentinel Hub: Modified Copernicus Sentinel data 2022/Sentinel Hub, <https://www.sentinel-hub.com> (last access: 19 January 2023), 2022.
- Shepherd, A., Ivins, E., Rignot, E., Smith, B., van Den Broeke, M., Velicogna, I., Whitehouse, P., Briggs, K., Joughin, I., Krinner, G., et al.: Mass balance of the Greenland Ice Sheet from 1992 to 2018, *Nature*, 579, 233–239, 2020.
- Sohn, H.-G., Jezek, K. C., and Van der Veen, C. J.: Jakobshavn Glacier, West Greenland: 30 years of spaceborne observations, *J. Geophys. Res.*, 25, 2699–2702, <https://doi.org/10.1029/98GL01973>, 1998.
- Stearns, L. A. and Hamilton, G. S.: Rapid volume loss from two East Greenland outlet glaciers quantified using repeat stereo satellite imagery, *Geophys. Res. Lett.*, 34, 5, <https://doi.org/10.1029/2006gl028982>, 2007.
- Sutherland, D. A., Straneo, F., and Pickart, R. S.: Characteristics and dynamics of two major Greenland glacial fjords, *J. Geophys. Res.-Oceans*, 119, 3767–3791, <https://doi.org/10.1002/2013jc009786>, 2014.
- Todd, J. and Christoffersen, P.: Are seasonal calving dynamics forced by buttressing from ice mélange or undercutting by melting? Outcomes from full-Stokes simulations of Store Glacier, West Greenland, *The Cryosphere*, 8, 2353–2365, <https://doi.org/10.5194/tc-8-2353-2014>, 2014.
- Walter, A., Lüthi, M. P., and Vieli, A.: Calving event size measurements and statistics of Eqip Sermia, Greenland, from terrestrial radar interferometry, *The Cryosphere*, 14, 1051–1066, <https://doi.org/10.5194/tc-14-1051-2020>, 2020.
- Walter, J. I., Box, J. E., Tulaczyk, S., Brodsky, E. E., Howat, I. M., Ahn, Y., and Brown, A.: Oceanic mechanical forcing of a marine-terminating Greenland glacier, *Ann. Glaciol.*, 53, 181–192, <https://doi.org/10.3189/2012aog60a083>, 2012.
- Wehrlé, A.: AdrienWehrle/earthspy: v0.3.0 (v0.3.0), Zenodo [code], <https://doi.org/10.5281/zenodo.7498876>, 2023a.
- Wehrlé, A.: earthspy Python package, GitHub [code], <https://github.com/AdrienWehrle/earthspy>, last access: 19 January 2023b.
- Wehrlé, A.: Greenland_ice_melange, Zenodo [data set], <https://doi.org/10.5281/zenodo.7499245>, 2023c.
- Wehrlé, A., Lüthi, M. P., Walter, A., Juvet, G., and Vieli, A.: Automated detection and analysis of surface calving waves with a terrestrial radar interferometer at the front of Eqip Sermia, Greenland, *The Cryosphere*, 15, 5659–5674, <https://doi.org/10.5194/tc-15-5659-2021>, 2021.
- Weidick, A. and Bennike, O.: Quaternary glaciation history and glaciology of Jakobshavn Isbræ and the Disko Bugt region, West Greenland: a review, Tech. Rep. 14, Geological Survey of Denmark and Greenland Bulletin, ISBN 978-87-7871-207-3, 2007.
- Williams, J. J., Gourmelen, N., Nienow, P., Bunce, C., and Slater, D.: Helheim Glacier Poised for Dramatic Retreat, *Geophys. Res. Lett.*, 48, e2021GL094546, <https://doi.org/10.1029/2021gl094546>, 2021.
- Xie, S., Dixon, T. H., Holland, D. M., Voytenko, D., and Vaňková, I.: Rapid Iceberg Calving Following Removal of Tightly Packed Pro-Glacial mélange, *Nat. Commun.*, 10, 3250, <https://doi.org/10.1038/s41467-019-10908-4>, 2019.